

Article

Influence of Fineness of Wheat Straw Ash on Autogenous Shrinkage and Mechanical Properties of Green Concrete

Muhammad Nasir Amin ^{1,2,*}, Muhammad Armaghan Siffat ³, Khan Shahzada ³ and Kaffayatullah Khan ^{1,2}

¹ Al Bilad Bank Scholarly Chair for Food Security in Saudi Arabia, the Deanship of Scientific Research, the Vice Presidency for Graduate Studies and Scientific Research, King Faisal University, Al-Ahsa 31982, Saudi Arabia; kghan@kfu.edu.sa

² Department of Civil and Environmental Engineering, College of Engineering, King Faisal University, Al-Ahsa 31982, Saudi Arabia

³ Department of Civil Engineering, University of Engineering and Technology, Peshawar 25120, Pakistan; ms12pwciv3699@uetpeshawar.edu.pk (M.A.S.); khanshahzada@uetpeshawar.edu.pk (K.S.)

* Correspondence: mgadir@kfu.edu.sa; Tel.: +966-13-589-5408; Fax: +966-13-581-7068

Abstract: This study investigates the effectiveness of an agricultural by-product wheat straw ash (WSA) as an internal curing agent in reducing the autogenous shrinkage of high-performance concrete (HPC). After incineration under different controlled time–temperature conditions, grinding and sieving were performed to obtain two different grades of fine WSA (F-WSA) and superfine WSA (SF-WSA). Subsequently, material characterization tests were carried out, followed by tests for mechanical properties and autogenous shrinkage potential of concrete incorporating 10% and 20% F-WSA and SF-WSA as a partial replacement of cement. The results demonstrated slightly higher compressive and tensile strength of concrete containing SF-WSA compared to control, whereas concrete with F-WSA demonstrated comparable strength results to that of the control concrete. Moreover, a significant reduction in 7 days' autogenous shrinkage was observed in concrete containing 10% and 20% F-WSA by 42% and 25% compared to that of control concrete, respectively. This reduction in autogenous shrinkage increased further to 57% and 40% for concrete with 10% and 20% SF-WSA, respectively. The results of microstructural investigations on paste samples such as FTIR, TGA, and N₂ adsorption analyses revealed a more refined and compact microstructure of paste samples with increasing fineness of WSA due to the formation of a more densified C-S-H phase. The improvement of the microstructure is attributable to the improved pozzolanic properties of SF-WSA compared with F-WSA.

Keywords: wheat straw ash; high-performance concrete; compressive and tensile strength; autogenous shrinkage; thermogravimetric analysis; Fourier transform infrared spectroscopy analysis; nitrogen adsorption



Citation: Amin, M.N.; Siffat, M.A.; Shahzada, K.; Khan, K. Influence of Fineness of Wheat Straw Ash on Autogenous Shrinkage and Mechanical Properties of Green Concrete. *Crystals* **2022**, *12*, 588. <https://doi.org/10.3390/cryst12050588>

Academic Editor: José L. García

Received: 8 March 2022

Accepted: 13 April 2022

Published: 22 April 2022

Publisher's Note: MDPI stays neutral with regard to jurisdictional claims in published maps and institutional affiliations.



Copyright: © 2022 by the authors. Licensee MDPI, Basel, Switzerland. This article is an open access article distributed under the terms and conditions of the Creative Commons Attribution (CC BY) license (<https://creativecommons.org/licenses/by/4.0/>).

1. Introduction

Concrete is the second most widely used material on earth after water. It is one of the most important components of our built environment and has numerous applications. The annual consumption of concrete is estimated at 30 billion tons [1,2]. Concrete is an ideal building material for infrastructure development due to its durability, strength, flexibility, and affordability [3,4]. However, its immense production results in a significant carbon footprint, contributing to 8% of global CO₂ emissions. Being a vital ingredient of concrete, the cement industry alone is responsible for 7% of the world's CO₂ emissions [5–7]. Such enormous CO₂ emissions contribute vastly to global warming and climate change [8,9]. Currently, there is increasing demand for low-carbon concrete for the mitigation and adaptation of climate change. There are a variety of technologies available, however the most suitable and practical for the ready-mix industry is the substitution of clinker, the major source of CO₂ emissions, with alternative natural/industrial pozzolanic or

cementitious materials [10–14]. Today, there are a variety of pozzolanic and supplementary cementitious materials (SCMs) available, such as fly ash [15], slag [16], silica fume [17], volcanic ash [18], agro by-product [19], stone industry waste [20], natural pozzolans [21], and so on, which can be used to partially replace cement clinkers. This consequently reduces the demand of cement and thus the CO₂ emissions. A number of factors can influence the ability of SCMs to gain traction in the future cement industry, including their availability, annual production levels, cost-effectiveness, and engineering characteristics. Therefore, there is an urgent need to explore new cement substitutes to fulfil the concrete industry's demands for reducing CO₂ emissions.

High-performance concrete (HPC) is widely accepted as a standard Portland cement concrete replacement owing to its workability, desired stability, and low-permeability characteristics [22]. Formation of HPC includes the use of very low water-to-binder (w/b) ratio with incorporation of chemical and mineral admixtures, i.e., rice husk ash (RHA), wheat straw ash (WSA), silica fume, super plasticizer, and so on [23]. Even though low w/b ratio together with admixtures yields high strength and durable concrete, a simultaneous drop in internal relative humidity leads to self-desiccation, which consequently causes autogenous shrinkage [24]. This is because a sudden drop in internal humidity owing to hydration generates a need for more water, because of which tiny capillaries appear on concrete surface [25]. This may lead to premature cracking of HPC and thus may allow harmful substances to possibly diffuse from the external environment into the internal matrix of concrete. As a result, the intended properties and life span of HPC structures will be greatly threatened [26]. On the other hand, drying shrinkage phenomena are not considered in such HPC due to a negligible evaporation from the surface of concrete. At the initial ages of casting, the vulnerability of concrete cracking due to autogenous shrinkage is of great concern to researchers.

For the mitigation of autogenous shrinkage, traditional external remedies such as curing and wet coating are insufficient to achieve required effects, owing to a relatively low surface permeability [27]. Hence, many investigators have suggested the uses of internal curing agents such as lightweight aggregates, absorbent limestone aggregates and absorbent polymers to control autogenous shrinkage and validate their efficiency [28,29]. However, use of these internal curing agents is not considered effective due to their high cost, difficulty in procuring and negative influence on the microstructural characteristics of concrete [30,31]. On the other hand, some researchers suggest the use of fine porous powders to reduce autogenous shrinkage, such as stone powder, bentonite clay, cenospheres, WSA and RHA [32,33]. The use of these inexpensive fine porous powders has resulted in controlling early age shrinkage due to their superfine, tiny structure and comparatively large surface area, able to enhance water absorbing capacity [34]. Many researchers have demonstrated the beneficial role of RHA in reducing autogenous shrinkage in developing HPC [35–37]. Therefore, there is a need to also investigate the effect of other agro wastes, such as bagasse ash and WSA, on the properties of HPC.

The secondary uses of these agricultural wastes are inevitable due to their associated environmental and landfill issues. Various power plants use some of these wastes as fuel and thus generate wasteful ashes. The dumping of these ashes into open fields, resulting from burning outside, has severe environmental and health implications. The construction industry has introduced a variety of agricultural wastes as potential substitutes for cement clinker in an effort to promote green construction and reduce air pollution. There have been several studies conducted over the last few decades on the possible uses of agro wastes in construction, such as sugar cane bagasse ash or RHA. Researchers found these ashes to be good pozzolanic materials due to their high content of amorphous silica [38–41]. Like sugarcane and rice, wheat is one of the main sources of food for 2.5 billion people in the world [42]. Globally, wheat production was estimated to be 750 million tons between 2016 and 2017. Among many, Pakistan is one of the world's largest wheat producers, as its production was estimated to be 26.6 million tons from 2017 to 2018 [43]. Saudi Arabia is one of the major wheat-producing countries in the Gulf region. The annual

wheat production of the Kingdom of Saudi Arabia is estimated to be 700,000 Tons [44]. According to Pan and Sano [45], the amount of wheat straw produced by one kg of wheat grain is approximately 1.3 to 1.4 kg. Most of this wheat straw is used as cattle feed [46]. In some cases, however, burning wheat straw in open fields causes air pollution (smog) and health problems for residents [47,48]. Many researchers have been investigating the role of WSA as an alternative cementitious material within cement and concrete, and have demonstrated improved mechanical properties of concrete containing around 20% of WSA [49–51]. However, it is still vital to increase understanding of WSA's optimal use for developing HPC. Thus, this study aims at enhancing scientific understanding and improving knowledge by evaluating the influence of the fineness of WSA on the mechanical and microstructural properties of concrete. A unique aspect of this research is to investigate how the fineness of WSA affects the behavior of autogenous shrinkage in high-strength concrete. This work is focused on optimizing the use of WSA in concrete production to produce more durable, sustainable, and stronger concrete.

In view of the above, there is still a need to investigate the influence of WSA origin, burning temperature, grinding cycles and so on, in reducing the autogenous shrinkage of HPC. Therefore, this study is conducted on a locally available wheat straw, considering its socio-economic and mechanical benefits. At first, the chemical composition of ground WSA was investigated using XRF, XRD and FTIR analyses to identify different phases present in WSA to understand the effect of both fine WSA (F-WSA) and superfine WSA (SF-WSA) on the strength, microstructure and shrinkage potential of HPC. Finally, the results of autogenous shrinkage, strength (compressive and tensile), and micro-structural characteristics (FTIR, TGA and BET analyses) of concrete with F-WSA and SF-WSA were presented and compared to those of control concrete (CC) with 100% cement.

2. Materials and Methods

2.1. Materials

In this study, a locally sourced type I ordinary Portland cement (OPC), complying with ASTM C150, was used as a chief binding material. The main physical and chemical composition of the cement is given in Table 1.

Table 1. Physical and chemical composition of the cement and wheat straw ash.

	OPC	WSA
Physical properties		
Specific gravity (g/cm ³)	3.15	2.21
Fineness (m ² /kg) (Blain)	344	-
Chemical properties (oxides, % by weight)		
SiO ₂	20.9	65.1
Al ₂ O ₃	5.18	9.10
Fe ₂ O ₃	3.04	2.67
(SiO ₂ + Al ₂ O ₃ + Fe ₂ O ₃) *	-	76.87
CaO	63.9	5.90
MgO	1.65	1.11
Na ₂ O	0.10	0.40
K ₂ O	0.52	10.5
SO ₃	2.61	1.13
LOI **	2.51	4.03
Compounds (%)		
C ₂ S	52.1	-
C ₃ S	19.6	-
C ₃ A	8.17	-
C ₄ AF	8.81	-

* ASTM C618-15; ** LOI = loss on ignition.

Locally available wheat straw used in this research was obtained from Khyber Pakhtunkhwa to produce HPC specimens. The duration and range of burning of WSA is very significant in defining the phases of amorphous and crystalline silica. Pervious research [49,50] has shown that the burning of wheat straw at low temperature results in the formation of high amount of amorphous silica in the WSA sample. Therefore, the wheat straw was burned at 550 °C for 4 h in a rotary kiln (Figure 1a). After incineration, WSA was subjected to grinding for 2 h in a rotary ball mill (Figure 1b) to obtain F-WSA. The F-WSA was further ground at 550 rpm for 3 h in a Planetary Mono Mill PULVERISETTE 6 (Figure 1c) to obtain SF-WSA. The purpose of obtaining two different finesses' of WSA (F-WSA and SF-WSA) was to evaluate the impact of high fineness on the engineering properties of HPC. The identification of the major traces of range of elements present in WSA are listed in Table 1. The mineral phases of WSA were then evaluated by XRD and FTIR analyses, as shown in Figure 2.

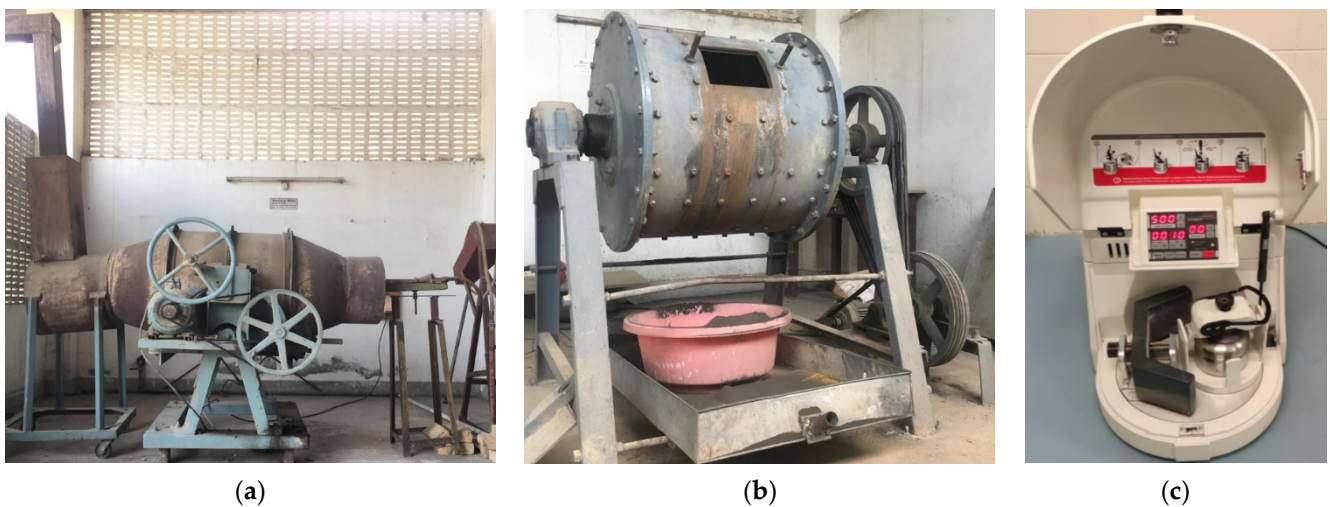


Figure 1. (a) Burning of WSA in a rotary kiln at 500 °C for 4 h, (b) rotary ball mill used in WSA grinding to obtain F-WSA, and (c) Planetary Mono Mill PULVERISETTE 6 used in F-WSA grinding to obtain SF-WSA.

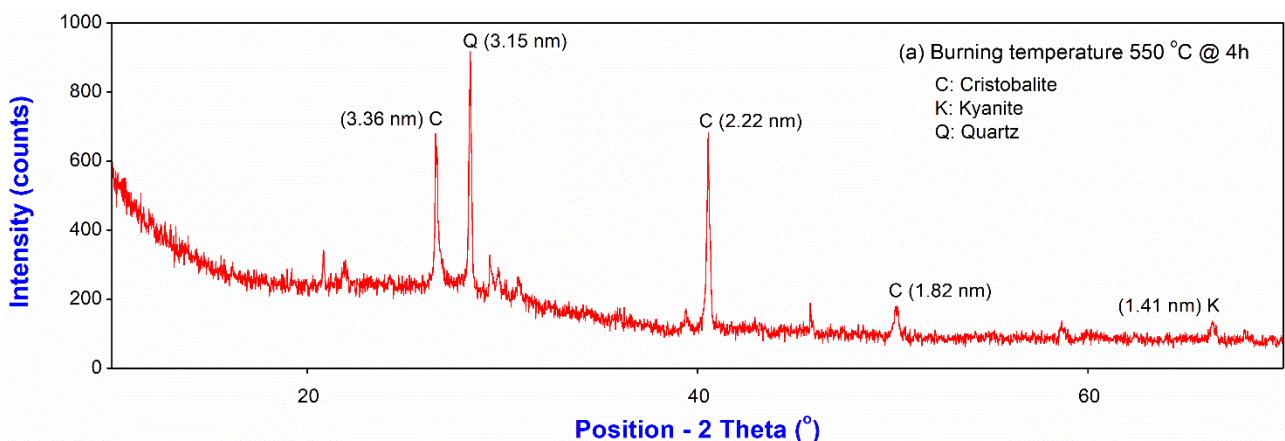


Figure 2. Cont.

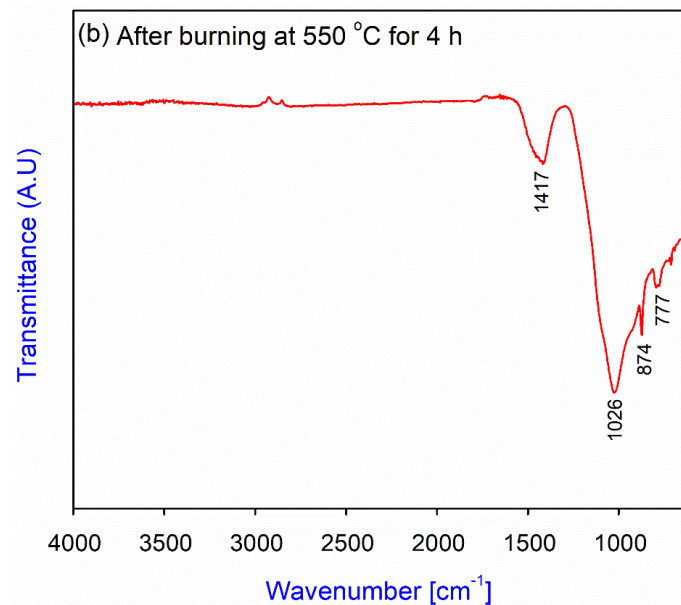


Figure 2. (a) XRD pattern, and (b) FTIR analysis results of WSA after heat treatment at 550 °C for 4 h.

In addition to binder materials, coarse and fine aggregates were procured from a local supplier. The maximum size of blended (50% was 20 mm down and 50% was 10 mm down) coarse aggregate used in this study was 20 mm. The sieve analysis tests were introduced to dry samples of both fine and coarse aggregates according to ASTM C136 (Table 2). The gradation curves of both fine and coarse aggregates are shown in Figure 3. The bulk density and water absorption of coarse aggregates were 1650 kg/m³ and 0.82%, respectively, along with specific gravity of 2.65 and Los Angeles Abrasion value 20.8%. Similarly, fine aggregate from a locally available source was obtained with specific gravity and water absorption values of 2.60 and 1.03%, respectively. The fineness modulus of fine aggregate was calculated as 2.54 (Table 2).

Table 2. Sieve analysis results of coarse and fine aggregates (ASTM C136).

Sieve #	Sieve Size (mm)	Weight Retained (g)	Weight Retained (%)	Cumulative Passing (%)	Cumulative Retained (%)
Coarse aggregate (CA)					
1 inch	25	0	0	100	0
3/4 inch	19	0	0	100	0
1/2 inch	12.5	1552	50.5	50	50
3/8 inch	9.5	803	26.1	23	77
No. 4	4.75	719	23.4	0	100
Fine aggregate (FA)					
3/8 inch	9.5	0	0	100	0
No. 4	4.75	0	0	100	0
No. 8	2.36	27	4.54	95.46	4.54
No. 16	1.18	96	16.1	79.33	20.67
No. 30	0.600	184	30.9	48.40	51.60
No. 50	0.300	157	26.4	22.02	77.98
No. 100	0.150	127	21.3	0.67	99.33
Pan		4	0.67	-	-
Fineness Modulus of FA (FM) = (0 + 4.54 + 20.67 + 51.6 + 77.98 + 99.33)/100 = 2.54					

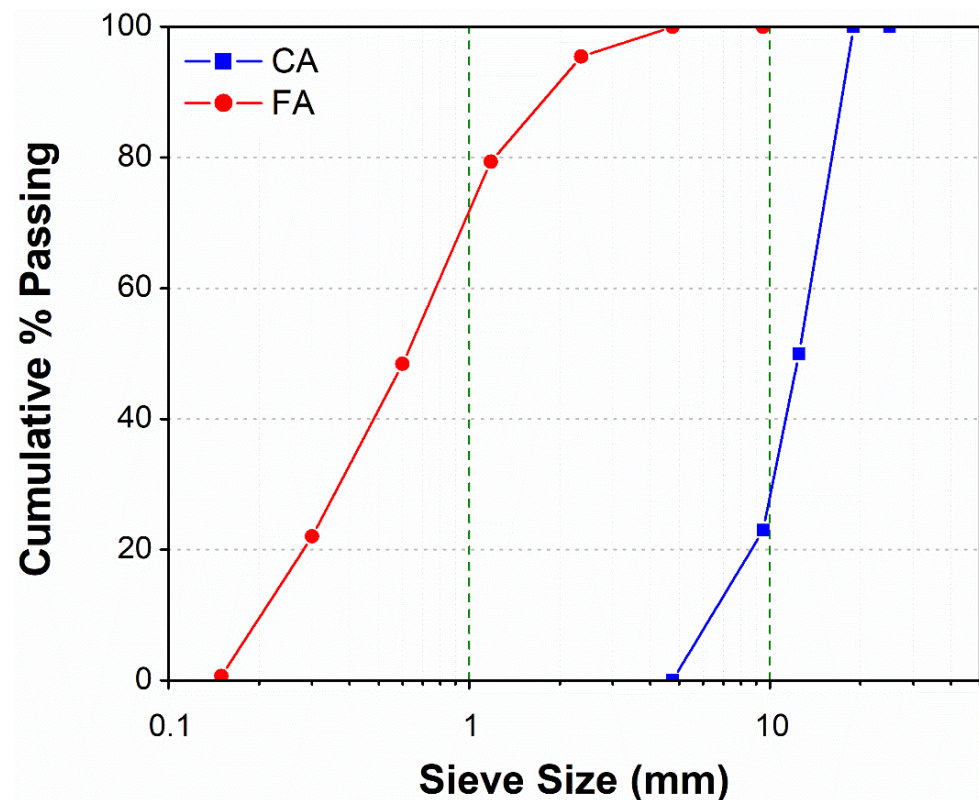


Figure 3. Grain size distribution of coarse and fine aggregates.

2.2. Mix Proportions and Methods

2.2.1. Concrete Mixture Proportions

Including control, five different concrete mixture proportions were selected. As listed in Table 3, the CC contains 100% cement, whereas the other four binary mixes contain 10% and 20% F-WSA and SF-WSA as a partial substitute of cement (F-WSA10, F-WSA20, SF-WSA10 and SF-WSA20). Detail of the concrete ingredients of each mixture is given in Table 3. A constant w/b ratio of 0.35 was maintained for all the concrete mixes. The targeted workability corresponding to slump values of 120 ± 30 mm was achieved by employing various percentages (wt.% binder) of a polycarboxylate-based high-range water-reducing admixture (Glenium 110M), complying with ASTM C494. Table 4 shows the basic characteristics of Glenium 110M admixture used in this study.

Table 3. Mixture proportions of concrete samples for compressive and tensile tests, and autogenous shrinkage (w/b = 0.35; a/b = 3.37; s/a = 0.40).

Mix ID	W (kg/m ³)	Binder, b (kg/m ³)			Aggregates, a (kg/m ³)		Slump (mm)
		C	F-WSA	SF-WSA	FA (S)	CA 10 mm	
Control concrete (C-100)		457	-	-			
Concrete containing 10% fine WSA (F-WSA10)	160	411	46	-	617	462	462
Concrete containing 20% fine WSA (F-WSA20)		366	91	-			
Concrete containing 10% superfine WSA (SF-WSA10)		411	-	46			
Concrete containing 20% superfine WSA (SF-WSA20)		366	-	91			

Table 4. The basic characteristics of Glenium 110M admixture.

Type	Characteristics
Color	Dark brown liquid
Specific gravity	1.065
Density	1.23 kg/liter
Storage provisions	Store in original containers at above 5 °C and below 30 °C
Dosage	1.7–2.0 L per 100 kg of cement
pH value	5.5
Solubility in water	Total
Physiological effect	Non-irritant

2.2.2. Concrete Mixing and Preparation of Test Specimens

A power-driven rotating pan mixer was used to mix the concrete ingredients, in accordance with the guidelines given by ASTM C192. For each concrete mixture, as shown in Table 3, immediately after mixing and testing to achieve the target slump, twelve cylindrical concrete specimens (100 mm diameter × 200 mm height) were cast according to the standard test method specified by ASTM C39. This is to test three identical specimens to determine average compressive and splitting tensile strengths at two different ages (7 and 28 days). After fabrication, the cylindrical molds were covered by plastic sheets and stored under standard laboratory temperature (20 ± 1 °C) and relative humidity ($60 \pm 5\%$) for 24 h. All the concrete specimens were demolded after 24 h of casting, followed by continuous moist curing in a water tub until testing ages. Upon reaching the desired curing period, both the upper and the lower ends of the cylindrical concrete specimens for compression tests were smoothly levelled by applying gypsum capping as per ASTM C617.

In addition to cylindrical specimens, prismatic concrete beam (500 mm × 100 mm × 100 mm) specimens were cast for all the concrete mixtures to directly measure their autogenous shrinkage (micro-strain) potentials using embedment strain transducer type EGP-5-120, with a grid resistance of $120 \pm 0.8\%$ Ohms and gauge factor of $2.03 \pm 1\%$ at 25 °C. As shown in Figure 4, an embedment strain transducer was placed in the center of specimen in the axial direction to measure the linear autogenous shrinkage of concrete specimens. After casting, the top surfaces of shrinkage specimens, while in the molds, were first wrapped with a water-proof polyethylene sheet, and then covered from the top followed by overlapping with aluminum foil. All the shrinkage specimens were securely stored under standard laboratory conditions of temperature (20 ± 1 °C) and relative humidity ($60 \pm 5\%$) for 24 h. After 24 h of casting, all the shrinkage specimens were demolded and entirely wrapped (all surfaces) with various layers of water-proof polyethylene sheeting, followed by covering with aluminum foil to ensure no moisture transport from the surfaces of concrete specimens.

2.3. Testing for Compressive Strength, Tensile Strength and Autogenous Shrinkage

The compression strength test was conducted on the cylindrical specimens as per ASTM C39 by deploying a 200-ton-capacity universal testing machine (UTM) assembly at a loading rate of 0.2 MPa/s. The split tensile test was conducted as per ASTM C496 by deploying a 200-ton UTM at a loading rate of 1 MPa/min. Figure 4 shows the test setup used to measure the compressive and tensile strength of concrete specimens.

After reaching to final setting time, the recording of micro-strain commences and continues for seven days uninterruptedly. As mentioned, the values of micro-strain were recorded continuously using a UCAM-70 data logger connected with MATLAB software. Figure 5 shows the experimental setup used to measure linear autogenous shrinkage of concrete specimens. For all concrete mixes, an average value of autogenous shrinkage was calculated to compare the results.



Figure 4. Test setup used to measure the compressive and tensile strength of concrete specimens.



Figure 5. Experimental setup used for measurement of autogenous shrinkage of concrete beams.

2.4. Casting and Curing of Paste Samples for Micro- and Pore-Structure Analysis

Paste specimens of control mix (100% cement) and the other binary mixes with 10% and 20% F-WSA and SF-WSA, as a partial replacement of cement (by weight), were prepared. For all mixes, a paste of standard consistency was prepared by mixing paste ingredients in a Hobart mixer. The mixture proportion of all paste specimens is given in Table 5. Immediately after mixing, the fresh cement pastes were poured into small plastic containers (diameter of 20 mm and height of 50 mm). Subsequently, the plastic containers were capped and sealed prior to curing. After 28 days in the cured state, the specimens were dried to inhibit the hydration process using the solvent exchange method. Finally, the flaky slices alongside the powder specimens were subjected to washing using isopropanol for 15 min. Afterwards, the paste samples were dried in an oven for 30 min at 40 °C to remove the isopropanol present in the samples, and the specimens were stored in sealed plastic bags until testing.

2.4.1. Nitrogen Adsorption Isotherm Technique

A N_2 sorptiometry study was conducted on the paste samples of all the studied concrete mixes. N_2 sorptiometry was used to characterize the surface area and pore structure of the powdered specimens (weighing approximately 0.3 g) obtained from the 28-days-cured hardened paste with a N_2 sorption analyzer (NOVA2200e, Quanta chrome, Boynton Beach, FL, USA) at 273 K. During the process, first, the specimens were degassed

to remove absorbed contaminants from the open air. Consequently, N₂ adsorption of the specimens was performed at ambient temperature and controlled pressure.

Table 5. Mixture proportion of control and other cement pastes containing F-WSA and SF-WSA.

Mix ID	Water (g)	Cement (g)	F-WSA (g)	SF-WSA (g)
C-100		200	0	0
F-WSA10		180	20	0
F-WSA20	80	160	40	0
SF-WSA10		180	0	20
SF-WSA20		160	0	40

2.4.2. Fourier-Transform Infrared Spectroscopy (FTIR) Analysis

The different phases of cement pastes were additionally characterized for all the studied mixes by performing FTIR analysis using a Perkin Elmer Spectrum Two FTIR spectrometer. The powdered samples of all the studied mixes obtained from 28-days-cured pastes were dried and subjected to an infrared light source, and the infrared spectra were recorded in the wavenumber range of 400 cm⁻¹ to 4000 cm⁻¹.

2.4.3. Thermogravimetric Analysis (TGA)

TGA was also conducted on the cement pastes by using Mettler Toledo instrument of all the studied mixes. The dried powdered specimens obtained from 28-days-cured pastes were placed inside the ceramic vessel of a thermal gravimetric analyzer. To dry the specimens, they were heated inside the thermal gravimetric analyzer to 20 to 1000 °C at a rate of 10 °C/min, with N₂ acting as the medium under static conditions. Additionally, alumina powder was incorporated as a reference to attain stability at elevated temperatures. Finally, the weight loss of various paste specimens in various temperature ranges was depicted by a comparison plot drawn using the built-in software.

3. Results and Discussions

3.1. Compressive and Tensile Strength of Concrete

Figure 6 shows a comparison of the compressive strength results of CC and concrete where cement was partially replaced with 10% and 20% of F-WSA and SF-WSA. The purpose of partially substituting cement with two different fineness's of WSA was to compare their results to those of the CC to determine the maximum possible replacement percentage of cement that does not compromise the strength and durability potentials. All the concrete specimens were water cured at a standard curing temperature of 20 °C until the age of testing.

The results show that the compressive strength of concrete containing 10% F-WSA was slightly reduced compared to CC at both 7 days and 28 days. However, compressive strength becomes closer and more comparable to CC with increasing cement substitution by 20% F-WSA. The lower strength of F-WSA10 than CC is due to its lower degree of pozzolanic activity, whereas a slight improvement of compressive strength of F-WSA20 demonstrates an enhancement of pozzolanic activity of the cementitious matrix. The above results suggested an addition of 20% F-WSA as an optimum cement replacement amount without compromising on the compressive strength of concrete. Unlike concrete containing F-WSA, the compressive strength of concrete containing SF-WSA increased both for 10% and 20% cement substitutions. This is due to an increased early age hydration rate and better packing and filling abilities along with the later-age pozzolanic reaction due to an increased fineness of SF-WSA compared to F-WSA. However, contrary to F-WSA, the compressive strength of concrete reduced with increasing percentage of SF-WSA from 10% to 20%. For instance, a 10% cement substitution with SF-WSA resulted in higher 7-day and 28-day compressive strength compared to the corresponding F-WSA10 concrete, as well as CC and F-WSA20. The results showed 5.7% and 6% increased strength of SF-WSA10

compared to CC at 7 days and 28 days, respectively. Moreover, the compressive strength of 20% SF-WSA concrete also remained higher compared to that of CC by 4.7% and 4.1% at 7 days and 28 days, respectively. This is attributed to increased fineness of WSA which resulted in high surface area and thus increased the pozzolanic reactivity of WSA [50,52]. Consequently, the above results demonstrate a positive impact of increasing fineness of WSA on the compressive strength of concrete.

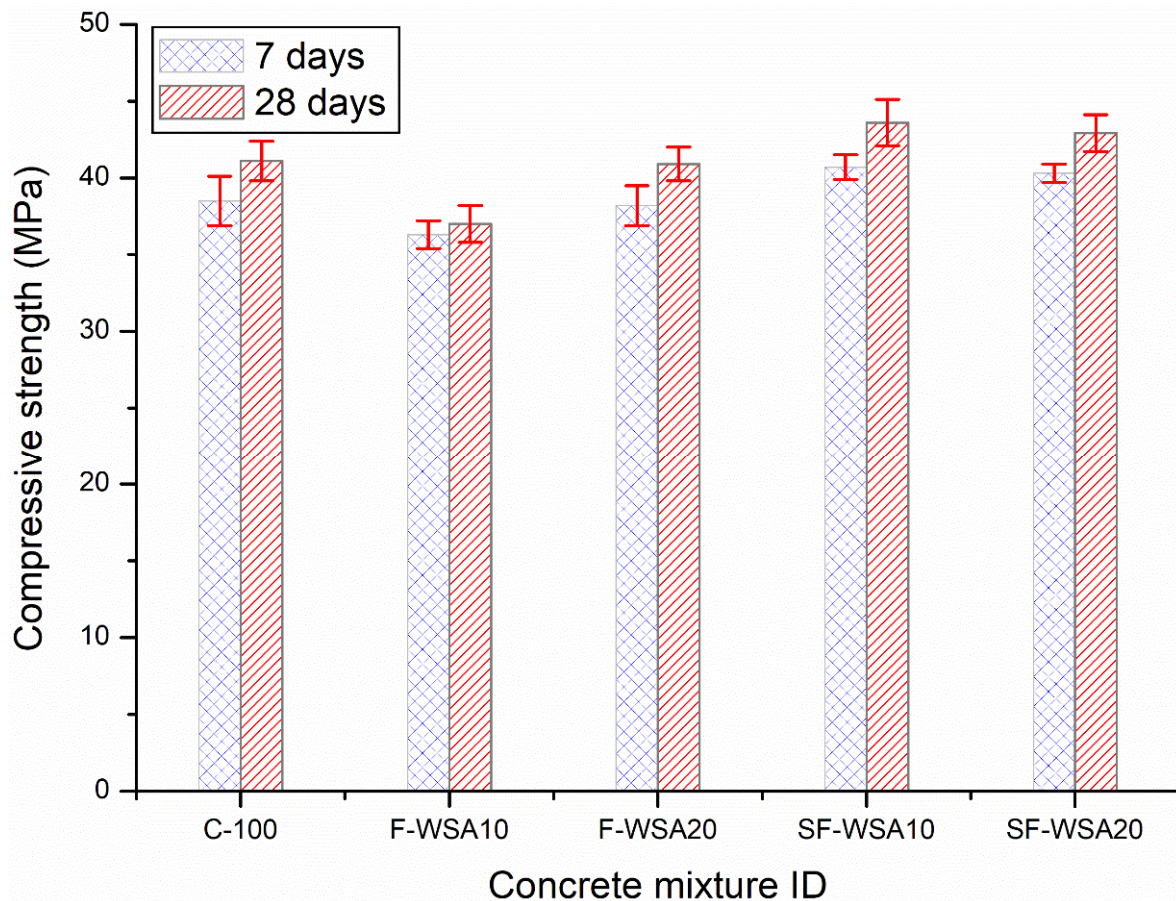


Figure 6. Comparison of 7-day and 28-day compressive strength development between control and concrete containing F-WSA and SF-WSA.

Like compressive strength, concrete containing 10% and 20% F-WSA demonstrated a slightly lower and comparable splitting tensile strength compared to CC, respectively. (Figure 7). However, with increasing fineness of WSA, splitting tensile strength compared to CC increased for both 10% and 20% cement substitution with SF-WSA. For instance, tensile strength of SF-WSA10 increased by 15% and 18.2% compared to CC at 7 days and 28 days, respectively. SF-WSA20 exhibited a respective 13.4% and 10.2% higher tensile strength compared to CC at 7 days and 28 days. The above, similar trends of both compressive and tensile strengths with respect to aging, percentage substitution of cement, and fineness of WSA, suggest a direct relationship between compressive and tensile strength of concrete.

3.2. Effect of Fineness of WSA on Autogenous Shrinkage of Concrete

Figure 8 shows a comparison of linear autogenous shrinkage between control and concretes containing 10% and 20% F-WSA and SF-WSA. For each concrete, the readings of micro-strain were directly obtained by using concrete embedment strain transducer without applying any thermal compensation. This is because very thin sized prismatic concrete beam specimens were used in measurement of shrinkage, where the temperature gradient across the cross-section remains close to a constant value [53]. In addition, all the

concrete beams were completely wrapped with a plastic sheet, over which another cover of aluminum foil was provided to avoid any moisture transportation.

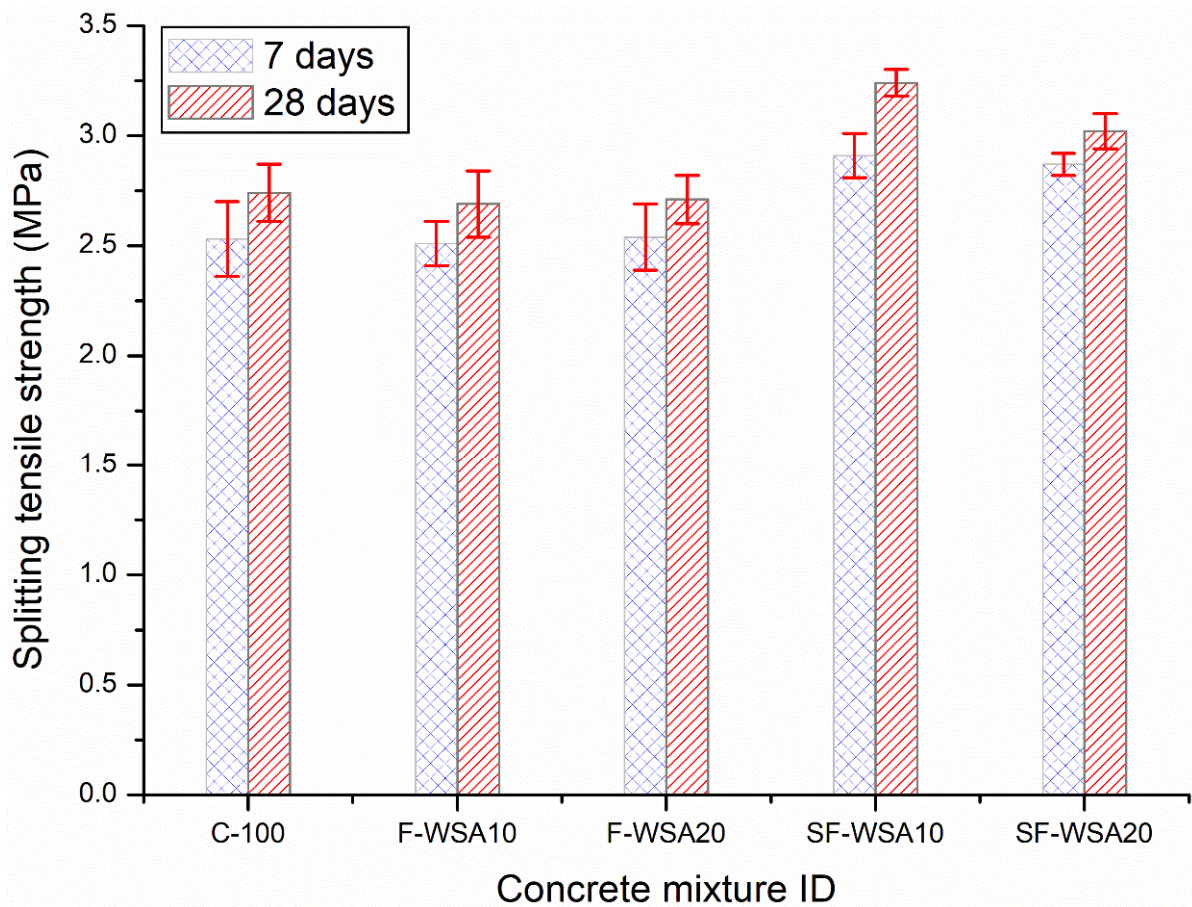


Figure 7. Comparison of 7-day and 28-day splitting tensile strength development between control and concrete containing F-WSA and SF-WSA.

Figure 8a shows that CC exhibited the highest amount of ultimate autogenous shrinkage (at 7 days) and a comparatively higher rate of early age autogenous shrinkage development among all concrete mixtures. From the comparison of autogenous shrinkage results, it is evident that both the rate as well as the ultimate autogenous shrinkage reduced owing to incorporation of WSA, whether it was fine or superfine. However, in addition to percentage cement substitution, a profound role of fineness of WSA in mitigating ultimate autogenous shrinkage was also observed. For instance, ultimate autogenous shrinkage of concrete with 10% and 20% F-WSA was reduced to 58% and 75% that of CC, respectively, as the ultimate autogenous shrinkage of CC was 201μ at 7 days (Figure 8b). A further reduction in autogenous shrinkage with increasing fineness of WSA was observed as 43% and 60% of CC for 10% and 20% SF-WSA, respectively. The current results demonstrated a promising role of WSA in mitigating overall autogenous shrinkage by acting as a source of an internal reservoir, thus leading to lowering of potential early age cracking. Moreover, the lowest autogenous shrinkage was observed corresponding to incorporation of 10% SF-WSA (87μ), which is attributed to improved fineness and micro-cellular structure of WSA as it led WSA to absorb more water from the mix, and consequently acted as an internal curing agent during the hydration reaction.

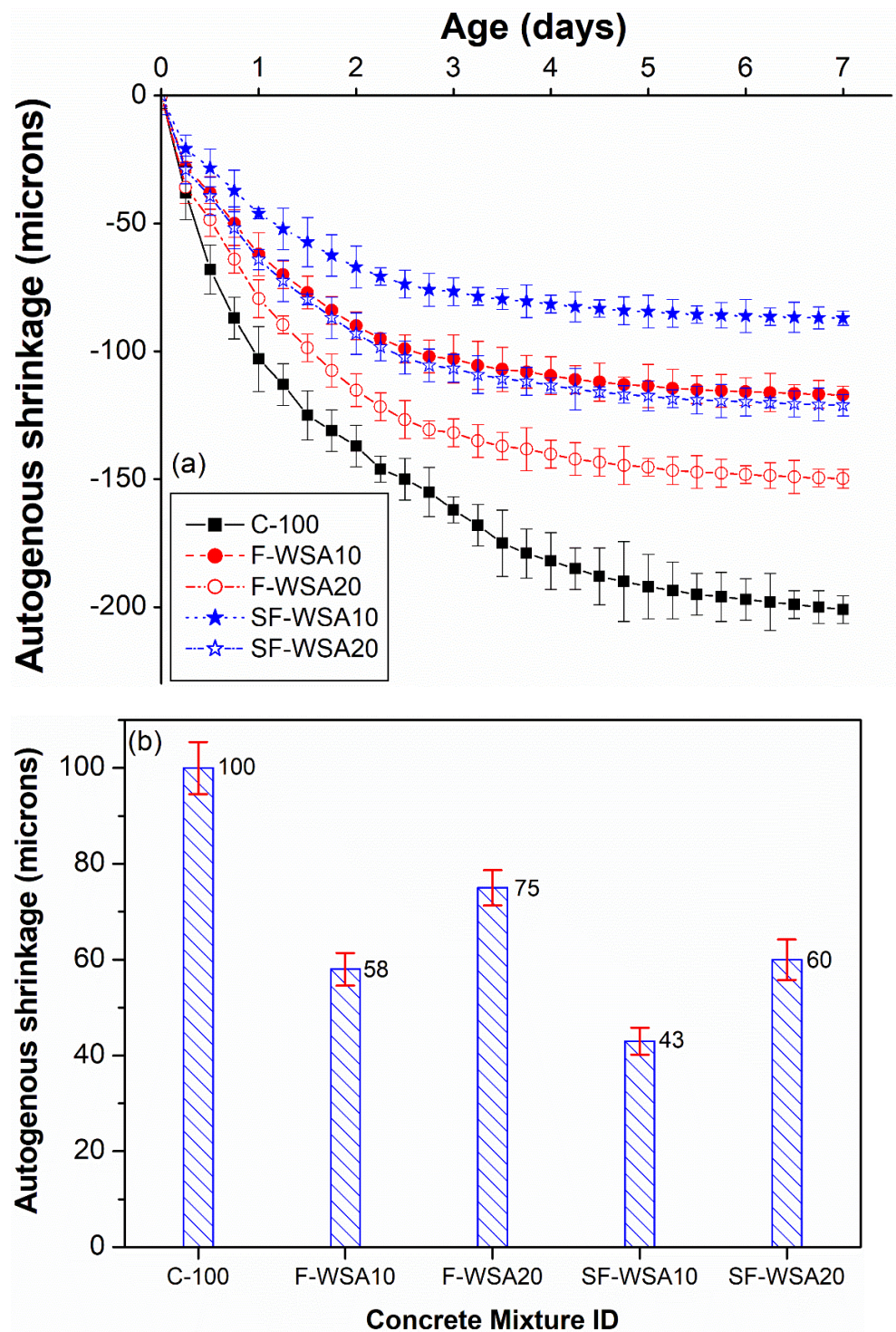


Figure 8. (a) Comparison of autogenous shrinkage of CC and binary concrete mixture containing 10% and 20% F-WSA and SF-WSA; (b) Normalized autogenous shrinkage of WSA concretes as a percentage of CC.

3.3. Fourier-Transform Infrared Spectroscopy (FTIR) Analysis of Cement Pastes Containing Fine and Superfine WSA

As illustrated in Figure 9, all the paste samples show that IR bands appeared at the same location, however, with different intensities. All cement blended samples demonstrated a primary C-S-H and C-H gel band between 956 and 968 cm^{-1} that displayed Si-O stretching of the Q^2 tetrahedra according to the Ca/Si ratio [54]. The peaks be-

tween 900 cm^{-1} and 1100 cm^{-1} are attributed to the vibrations of Si-O bonds in the C-S-H phase [55]. The shift in the Si-O band toward a high wavenumber is due to the polymerization of silica. The C-100 paste resulted in a 956 cm^{-1} peak value, whereas F-WSA10 and F-WSA20 demonstrated peaks of 961 cm^{-1} and 965 cm^{-1} , respectively. The samples of SF-WSA10 and SF-WSA20 showed summits of 968 cm^{-1} each. A shift toward a higher wavenumber in the spectra of SF-WSA mixes suggests the formation of a high number of C-S-H gels. A large number of C-S-H gels might be produced from the nucleation sites provided by the fine particles of WSA. Furthermore, the peaks at 720 cm^{-1} , 875 cm^{-1} , and 1415 cm^{-1} are associated with calcite formed due to carbonation [56].

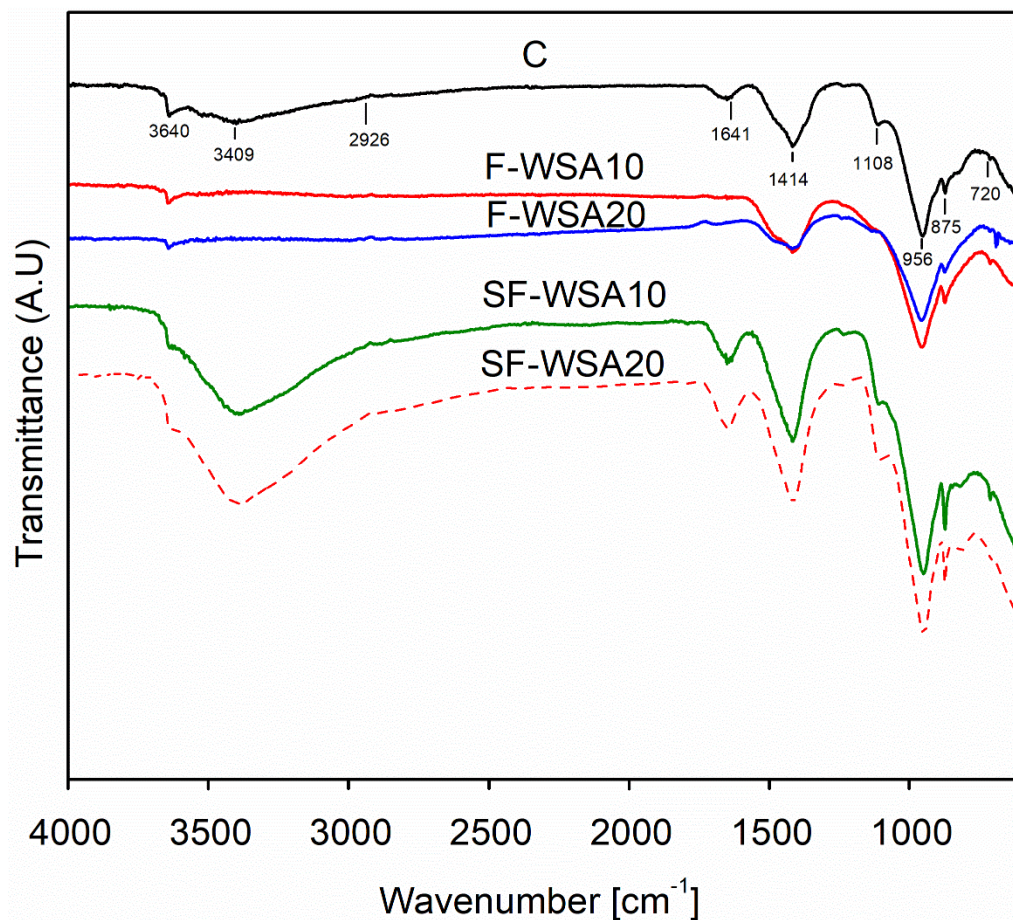


Figure 9. FTIR intensities for control concrete (CC) paste and pastes containing different percentages of fine and superfine WSA at 28 days.

In all the paste samples, the peak at 3645 cm^{-1} indicates the presence of free OH groups, which suggests the presence of the portlandite phase. The control sample exhibits a wider and more visible peak compared to all other binary samples. In addition, the portlandite peak for SF-WSA10 and SF-WSA20 remained very small, indicating a high pozzolanic reactivity, which consequently resulted in greater consumption of C-H. This led to formation of more C-S-H gels in these mixes.

3.4. Thermogravimetric Analysis (TGA) of Cement Pastes Containing Fine and Superfine WSA

According to Figure 10, the results of the TGA analysis conducted on a control paste and WSA-aided pastes for 28 days indicated the percentage of weight loss in the samples at different temperatures. The phases from 400 °C to 500 °C represent the breakdown of calcium hydroxide Ca(OH)_2 during the hydration reaction [57,58]. TGA analysis evaluates the consumption of Ca(OH)_2 with aging, and hence indicates the pozzolanic potential of the material [59]. The relative graph obtained from TGA analysis demonstrated that

the maximum amount of weight loss occurred in control specimen between 400 °C and 500 °C, which indicates the continuous formation of $\text{Ca}(\text{OH})_2$ during hydration phenomena. Contrarily, C-H content gradually decreases in binary mixes with increasing percent substitution of cement with WSA. The gradual decrease in C-H content in binary mixes is obviously due to their decreasing cement content, as well as partly due to the pozzolanic reactivity caused by WSA due to the formation of hydration products because of C-H consumption. However, compared to F-WSA10 and F-WSA20, the cement paste samples with SF-WSA10 and SF-WSA20 showed significant decreases in the C-H phase, which is due to the simultaneous effects of high reactivity of SF-WSA due to its very fine particle size. This led to high densification and compactness of the microstructure of C-S-H gel, and ultimately resulted in better engineering performance for mixes with superfine WSA.

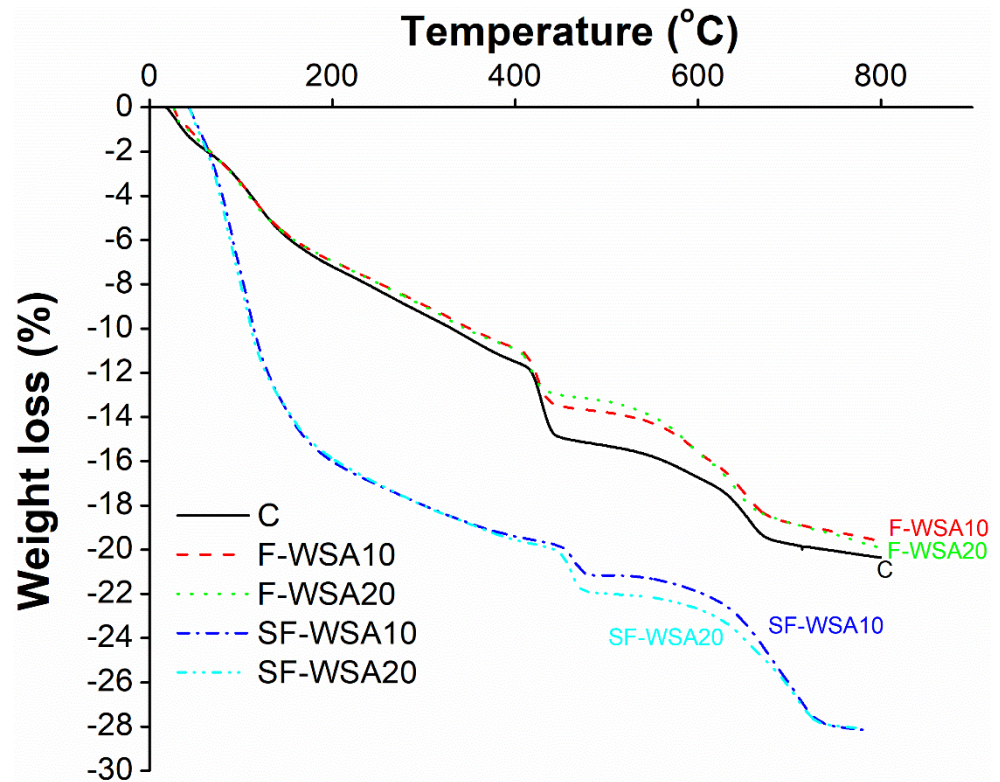


Figure 10. TGA results for control concrete (CC) paste and pastes containing different percentages of fine and superfine WSA at 28 days.

3.5. Nitrogen Adsorption Results (Surface Area and Pore Structure of Cement Pastes) of Cement Pastes Containing Fine and Superfine WSA

Table 6 shows the cumulative nitrogen intrusion volume and BET surface area for different paste samples after curing for 28 days. The lowest nitrogen intrusion volume ($0.043 \text{ cm}^3/\text{g}$) was observed for a binary mix with 20% cement substitution for SF-WSA20, followed by F-WSA20 ($0.045 \text{ cm}^3/\text{g}$), SF-WSA10 ($0.048 \text{ cm}^3/\text{g}$), F-WSA10 ($0.048 \text{ cm}^3/\text{g}$), and control ($0.049 \text{ cm}^3/\text{g}$). The relatively lower pore volume of SF-WSA20 mix indicates the formation of dense pore structure owing to accelerated pozzolanic reactivity caused by the highly reactive superfine WSA. In addition, the binary mixes with lower percent of WSA (F-WSA10 and SF-WSA10) exhibited lesser nitrogen intrusion volume compared to control; however, both these samples showed more nitrogen intrusion volume compared to samples with 20% of these materials. This is most obviously due to reduced pozzolanic reactivity because of the low amount of both F-WSA and SF-WSA in the cement matrix, which consequently led to increased porosity in the paste matrix.

Table 6. BET surface area and intruded pore volume for control (C-100) and other pastes containing F-WSA and SF-WSA.

Mix ID	BET Surface Area (m ² /g)	Intruded Pore Volume (cm ³ /g)
C-100	11.690	0.049
F-WSA10	11.796	0.048
F-WSA20	13.263	0.045
SF-WSA10	11.833	0.048
SF-WSA20	17.784	0.043

A comparison of Brunauer–Emmett–Teller (BET) surface areas between control and other binary mixes is presented in Table 6. All binary mixes exhibited higher BET surface areas compared to the control sample. Like for the lowest nitrogen intruded volume, SF-WSA20 demonstrated a higher BET surface area (17.748 m²/g) compared to all other mixes. An increased BET surface area of the SF-WSA20, indicates its improved and more dense microstructure of C-S-H gels [60,61]. Overall, the binary mixes with 20% WSA (F-WSA20 and SF-WSA20) showed increases in BET surface area compared to mixes with 10% of both fine and superfine WSA (F-WSA10 and SF-WSA10). These results show that the addition of 20% F-WSA and 20% SF-WSA led to increased pozzolanic reactivity, which caused formation of dense phases and pore structure and ultimately better engineering performance.

4. Conclusions

This study investigated the effect of fineness of a locally generated agriculture waste WSA on pozzolanic performance and mitigating autogenous shrinkage during early setting of HPC by acting as an internal curing agent. At first, WSA with a maximum amount of reactive silica in amorphous form was obtained from an optimized incinerating temperature (550 °C for 4 h) based on XRD and XRF analyses, followed by its extensive grinding by employing various cycles, achieving two different desired fineness's (fine and superfine passing # 200 sieve (75µ)). Finally, mix designs of CC (100% cement) and those containing 10% and 20% fine and superfine WSA as a partial substitute of cement were prepared. Subsequently, the influence of fineness of WSA was evaluated by performing tests for mechanical strength, shrinkage potential and microstructural investigations, and compared to those of CC.

The main findings of this study are summarized below:

- The current results demonstrated a slight reduction in compressive and tensile strengths for F-WSA10 (10% cement substitution) compared to CC, at 7 days as well as 28 days. However, with increasing cement substitution, F-WSA20 (20% cement substitution) showed close and comparable strengths to those of CC. Moreover, with increasing fineness of WSA, slight increases in 28-day compressive and tensile strengths were observed compared to those of CC by 6% and 18.2% for SF-WSA10, respectively, and by 4.1% and 10.2% for SF-WSA20, respectively. These improvements in strengths at 7 days were 5.7% and 15% for SF-WSA10 and 4.7% and 13.4% for SF-WSA20, respectively.
- These results demonstrated a promising role of incorporating WSA in minimizing rate as well as mitigation of ultimate autogenous shrinkage. It was found that ultimate autogenous shrinkage of concrete with 10% and 20% F-WSA was reduced to 58% and 75% of that of CC (201µ at 7 days), respectively. Moreover, with increasing fineness of WSA, the ultimate autogenous shrinkage further reduced to 43% and 60% of CC for 10% and 20% SF-WSA, respectively. This lower ultimate autogenous shrinkage is attributed to improved fineness and micro-cellular structure of WSA, which leads to absorption of more water from the mix and consequently acts as an internal curing agent during hydration reaction, which could ultimately prevent the formation of micro-cracks on the concrete surface.

- A quite visible shift in the Si-O band was observed through FTIR analysis for almost all the binary mixes containing either F-WSA or SF-WSA. However, comparatively, the shift was more pronounced in binary mixes containing SF-WSA (SF-WSA10 and SF-WSA20), which clearly demonstrates the presence of high levels of C-S-H gels. Moreover, the portlandite peaks (3641–3644 cm^{-1}) were also comparatively smaller in these mixes compared to other binary and control mixes. This consequently suggests improved pozzolanic reactivity and the formation of more C-S-H gels owing to high fineness of WSA.
- The results of N₂ adsorption tests indicate densification of the paste matrix and refinement of the pore structure due to a decrease in intruded pore volume and an increase in BET surface area for binary mixes with F-WSA and SF-WSA. Specifically, the binary mix containing 20% SF-WSA (SF-WSA20) showed the lowest intruded pore volume and high BET surface area, which indicates better pozzolanic reactivity of superfine WSA, ultimately causing densification and refinement of the pore structure of the paste matrix.
- TGA results also showed a reduction in the portlandite phase of binary mixes compared to the control sample. This happened especially in binary mixes with high doses of both fine and superfine WSA (F-WSA20 and SF-WSA20). This is partly because of the lower amount of cement in these mixes, as well as being due to the high pozzolanic reactivity of amorphous silica present in WSA, ultimately generating additional C-S-H phases and leading to densification of the paste matrix.

Author Contributions: M.N.A. and K.K. contributed to the design of this research. M.A.S. and K.S. contributed to performing the experiments starting with the collection of all materials, burning WSA in kiln, grinding, sieving WSA to obtain desired fineness's, mixing, casting, demolding, curing and mechanical testing. M.A.S. and K.K. supported in performing XRD, FTIR, TGA, and N₂ adsorption analyses of materials and pastes. M.N.A., M.A.S. and K.K. critically analyzed and discussed the results of this research and prepared an initial draft of this manuscript. M.N.A. prepared all Figures and Tables and prepared the final draft of this manuscript. All authors have read and agreed to the published version of the manuscript.

Funding: This work was supported by the Al Bilad Bank Scholarly Chair for Food Security in Saudi Arabia, the Deanship of Scientific Research, Vice Presidency for Graduate Studies and Scientific Research, King Faisal University, Saudi Arabia [Grant No. CHAIR77]. The APC was funded by the same "Grant No. CHAIR77".

Institutional Review Board Statement: Not applicable.

Informed Consent Statement: Not applicable.

Data Availability Statement: All the data utilized in current research are available upon a reasonable request from the corresponding author.

Acknowledgments: The authors acknowledge the Al Bilad Bank Scholarly Chair for Food Security in Saudi Arabia, the Deanship of Scientific Research, Vice Presidency for Graduate Studies and Scientific Research, King Faisal University, Saudi Arabia, for the financial support [Grant No. CHAIR77].

Conflicts of Interest: The authors declare no conflict of interest. The funding sponsors had no role in the design of the study; in the collection, analyses, or interpretation of data; in the writing of the manuscript, or in the decision to publish the results.

References

1. Yang, K.H.; Jung, Y.B.; Cho, M.S.; Tae, S.H. Effect of supplementary cementitious materials on reduction of CO₂ emissions from Concrete. In *Handbook of Low Carbon Concrete*, 1st ed.; Butterworth-Heinemann: Oxford, UK, 2017; pp. 89–110.
2. Klee, H. *The Cement Sustainability Initiative: Recycling Concrete-Summary*; WBCSD: Geneva, Switzerland, 2009.
3. Global Alliance for Buildings and Construction. *2020 Global Status Report for Buildings and Construction: Towards a Zero-Emission, Efficient and Resilient Buildings and Construction Sector*; United Nations Environment Programme: Nairobi, Kenya, 2020.
4. Organization for Economic and Co-operation and Development (OECD). *Global Material Resources Outlook to 2060*; OECD: Paris, France, 2018.
5. Barcelo, L.; Kline, J.; Walenta, G.; Gartner, E. Cement and carbon emissions. *Mater. Struct.* **2014**, *47*, 1055–1065. [[CrossRef](#)]

6. IEA; WBCSD. *Cement Technology Roadmap 2009: Carbon Emissions Reductions up to 2050*; OECD/IEA: Paris, France; WBCSD: Geneva, Switzerland, 2009.
7. WBCSD. *Cement Sustainability Initiative, Getting the Numbers Right, Project Emissions Report*; WBCSD: Geneva, Switzerland, 2016.
8. Solomon, S.; Plattner, G.-K.; Knutti, R.; Friedlingstein, P. Irreversible climate change due to carbon dioxide emissions. *Proc. Natl. Acad. Sci. USA* **2009**, *106*, 1704–1709. [[CrossRef](#)] [[PubMed](#)]
9. Scrivener, K.L.; John, V.M.; Gartner, E.M. Eco-efficient cements: Potential economically viable solutions for a low-CO₂ cement-based materials industry. *Cem. Concr. Res.* **2018**, *114*, 2–26. [[CrossRef](#)]
10. Hasanbeigi, A.; Price, L.; Lin, E. Emerging energy-efficiency and CO₂ emission-reduction technologies for cement and concrete production: A technical review. *Renew. Sustain. Energy Rev.* **2012**, *16*, 6220–6238. [[CrossRef](#)]
11. Habert, G.; Miller, S.A.; John, V.M.; Provis, J.L.; Favier, A.; Horvath, A.; Scriver, K.L. Environmental impacts and decarbonization strategies in the cement and concrete industries. *Nat. Rev. Earth Environ.* **2020**, *11*, 559–573. [[CrossRef](#)]
12. Van Vuuren, D.P.; Stehfest, E.; Gernaat, D.E.; Van Den Berg, M.; Bijl, D.L.; De Boer, H.S.; Daioglou, V.; Doelman, J.C.; Edelenbosch, O.Y.; Harmsen, M.; et al. Alternative pathways to the 1.5 C target reduce the need for negative emission technologies. *Nat. Clim. Change* **2018**, *8*, 559–573. [[CrossRef](#)]
13. Shi, C.; Qu, B.; Provis, J.L. Recent progress in low-carbon binders. *Cem. Concr. Res.* **2019**, *122*, 227–250. [[CrossRef](#)]
14. Hills, T.; Leeson, D.; Florin, N.; Fennell, P. Carbon capture in the cement industry: Technologies, Progress, and retrofitting. *Environ. Sci. Technol.* **2016**, *50*, 368–377. [[CrossRef](#)]
15. Marinković, S.; Dragaš, J. *Fly ash. Waste and Supplementary Cementitious Materials in Concrete: Characterisation, Properties and Applications*; Woodhead Publishing: Sawston, UK, 2018; pp. 325–360.
16. Gencil, O.; Karadag, O.; Oren, O.H.; Bilir, T. Steel slag and its applications in cement and concrete technology: A review. *Constr. Build. Mater.* **2021**, *283*, 122783. [[CrossRef](#)]
17. Khan, M.I.; Sutanto, M.H.; Napiah, M.B.; Khan, K.; Rafiq, W. Design optimization and statistical modeling of cementitious grout containing irradiated plastic waste and silica fume using response surface methodology. *Construct. Build. Mater.* **2021**, *271*, 121504. [[CrossRef](#)]
18. Khan, K.; Amin, M.N.; Saleem, M.U.; Qureshi, H.J.; Al-Faiad, M.A.; Qadir, M.G. Effect of Fineness of Basaltic Volcanic Ash on Pozzolanic Reactivity, ASR Expansion and Drying Shrinkage of Blended Cement Mortars. *Materials* **2019**, *12*, 2603. [[CrossRef](#)] [[PubMed](#)]
19. Raheem, A.A.; Ikotun, B.D. Incorporation of agricultural residues as partial substitution for cement in concrete and mortar—A review. *J. Build. Eng.* **2020**, *31*, 101428. [[CrossRef](#)]
20. Amin, M.N.; Khan, K.; Saleem, M.U.; Khurram, N.; Niazi, M.U.K. Aging and Curing Temperature Effects on Compressive Strength of Mortar Containing Lime Stone Quarry Dust and Industrial Granite Sludge. *Materials* **2017**, *10*, 642. [[CrossRef](#)] [[PubMed](#)]
21. Scrivener, K.; Martirena, F.; Bishnoi, S.; Maity, S. Calcined clay limestone cements (LC³). *Cem. Concr. Res.* **2018**, *114*, 49–56. [[CrossRef](#)]
22. Owaid, H.M.; Roszilah, H.; Abdullaha, S. Physical and Mechanical Properties of High Performance Concrete with Alum Sludge as Partial Cement Replacement. *J. Teknol.* **2013**, *65*, 105–112.
23. Jagtap, S.; Kareliya, K.H.; Ukarande, S.K. High Performance Concrete with Mineral Admixtures. *Int. J. Glob. Technol. Initiat.* **2015**, *4*, A80–A87.
24. Aili, A.; Vandamme, M.; Torrenti, J.-M.; Masson, B. Is long-term autogenous shrinkage a creep phenomenon induced by capillary effects due to self-desiccation. *Cem. Concr. Res.* **2018**, *108*, 186–200. [[CrossRef](#)]
25. Shen, D.; Liu, X.; Zeng, X.; Zhao, X.; Jiang, G. Effect of polypropylene plastic fibers length on cracking resistance of high-performance concrete at early age. *Constr. Build. Mater.* **2020**, *244*, 117874. [[CrossRef](#)]
26. Ma, Z.; Zhu, F.; Zhao, T. Effects of surface modification of silane coupling agent on the properties of concrete with freeze-thaw damage. *KSCE J. Civ. Eng.* **2018**, *22*, 657–669. [[CrossRef](#)]
27. Ye, G.; Nguyen, V.T. Mitigation of autogenous shrinkage of ultra-high-performance concrete by rice husk ash. *J. Chin. Ceram. Soc.* **2012**, *40*, 212–216.
28. Balapour, M.; Zhao, W.; Garboczi, E.J.; Oo, N.Y.; Spataro, S.; Hsuan, Y.G.; Billen, P.; Farnam, Y. Potential use of lightweight aggregate (LWA) produced from bottom coal ash for internal curing of concrete systems. *Cem. Concr. Compos.* **2020**, *105*, 103428. [[CrossRef](#)]
29. Aslam, M.; Shafiq, P.; Jumaat, M.Z. Structural Lightweight Aggregate Concrete by Incorporating Solid Wastes as Coarse Lightweight Aggregate. *Appl. Mech. Mater.* **2015**, *749*, 337–342. [[CrossRef](#)]
30. Zhang, M.-H.; Gjorv, O.E. Characteristics of lightweight aggregates for high-strength concrete. *ACI Mater. J.* **1991**, *88*, 150–158.
31. Dang, J.; Zhao, J.; Du, Z. Effect of Superabsorbent Polymer on the Properties of concrete. *Polymers* **2017**, *9*, 672. [[CrossRef](#)]
32. De Souza, F.B.; Montedo, O.R.K.; Grassi, R.L.; Antunes, E.G.P. Lightweight high-strength concrete with the use of waste cenosphere as fine aggregate. *Rev. Mater.* **2019**, *24*, e12509. [[CrossRef](#)]
33. Afzal, S.; Shahzada, K.; Fahad, M.; Saeed, S.; Ashraf, M. Assessment of early-age autogenous shrinkage strains in concrete using bentonite clay as internal curing technique. *Constr. Build. Mater.* **2014**, *66*, 403–409. [[CrossRef](#)]
34. Jensen, O.M.; Lura, P. Techniques and materials for internal water curing of concrete. *Mater. Struct.* **2006**, *39*, 817–825. [[CrossRef](#)]

35. Nguyen, V.T. Rice Husk Ash as a Mineral Admixture for Ultra High Performance Concrete. Ph.D. Thesis, Delft University, Delft, The Netherlands, 2011.
36. De Sensale, G.R.; Ribeiro, A.B.; Gonçalves, A. Effects of RHA on autogenous shrinkage of Portland cement pastes. *Cem. Concr. Compos.* **2008**, *30*, 892–897. [[CrossRef](#)]
37. Rizwan, S.A. High-Performance Mortars and Concretes Using Secondary Raw Materials. Ph.D. Thesis, Faculty of Maschinenbau, Verfahrens-und Energietechnik der Technischen Bergakademie Freiberg, Freiberg, Germany, 2006.
38. Cordeiro, G.C.; Toledo, R.D.; Tavares, L.M.; Fairbairn, E.M.R. Pozzolanic activity and filler effect of sugar cane bagasse ash in Portland cement and lime mortars. *Cem. Concr. Compos.* **2008**, *30*, 410–418. [[CrossRef](#)]
39. Rukzon, S.; Chindaprasirt, P. Utilization of bagasse ash in high-strength concrete. *Mater. Des.* **2012**, *34*, 45–50. [[CrossRef](#)]
40. Zhang, M.H.; Malhotra, V.M. High-performance concrete incorporating rice husk ash as supplementary cementing materials. *ACI Mater. J.* **1996**, *93*, 629–636.
41. Habeeb, G.A.; Fayyadh, M.M. Rice husk ash concrete: The effect of RHA average particle size on mechanical properties and drying shrinkage. *Aust. J. Basic Appl. Sci.* **2009**, *3*, 1616–1622.
42. FAO World Food Situation. Available online: <http://www.fao.org/worldfoodsituation/csdb/en/> (accessed on 20 October 2018).
43. Largest Wheat Producing Countries Worldwide in 2017/2018. Available online: <https://www.statista.com/statistics/237912/global-top-wheat-producing-countries/> (accessed on 20 October 2018).
44. Sadik, M.W.; El Shaer, H.M.; Yakot, H.M. Recycling of Agriculture and Animal Farm Wastes into Compost Using Com-post Activator in Saudi Arabia. *J. Int. Environ. Appl. Sci.* **2010**, *5*, 397–403.
45. Pan, X.; Sano, Y. Fractionation of wheat straw by atmospheric acetic acid process. *Bioresour. Technol.* **2005**, *96*, 1256–1263. [[CrossRef](#)]
46. Kadam, K.L.; Forrest, L.H.; Jacobson, W.A. Rice straw as a lignocellulosic resource: Collection, processing, transportation, and environmental aspects. *Biomass Bioenergy* **2000**, *18*, 369–389. [[CrossRef](#)]
47. Shazim, A.M.; Israr, W.; Muhammad, K.K.; Muhammad, A.T.; Madina, B. Environmentally Friendly Utilization of Wheat Straw Ash in Cement-Based Composites. *Sustainability* **2018**, *10*, 1322.
48. Binici, H.; Aksogan, O. The use of ground blast furnace slag, chrome slag and corn stem ash mixture as a coating against corrosion. *Constr. Build. Mater.* **2011**, *25*, 4197–4201. [[CrossRef](#)]
49. Biricik, H.; Aköz, F.; Berktaş, I.; Tulgar, A.N. Study of pozzolanic properties of wheat straw ash. *Cem. Concr. Res.* **1999**, *29*, 637–643. [[CrossRef](#)]
50. Amin, M.N.; Murtaza, T.; Shahzada, K.; Khan, K.; Adil, M. Pozzolanic Potential and Mechanical Performance of Wheat Straw Ash Incorporated Sustainable Concrete. *Sustainability* **2019**, *11*, 519. [[CrossRef](#)]
51. Khushnood, R.A.; Rizwan, S.A.; Memon, S.A.; Tulliani, J.-M.; Ferro, G.A. Experimental Investigation on Use of Wheat Straw Ash and Bentonite in Self-Compacting Cementitious System. *Adv. Mater. Sci. Eng.* **2014**, *2014*, 832508. [[CrossRef](#)]
52. Bheel, N.; Ali, M.O.A.; Kirgız, M.S.; De Sousa Galdino, A.G.; Kumar, A. Fresh and mechanical properties of concrete made of binary substitution of millet husk ash and wheat straw ash for cement and fine aggregate. *J. Mater. Res. Technol.* **2021**, *13*, 872–893. [[CrossRef](#)]
53. Perraki, T.; Kakali, G.; Kontoleon, F. The effect of natural zeolites on the early hydration of Portland cement. *Microporous Mesoporous Mater.* **2003**, *61*, 205–212. [[CrossRef](#)]
54. Yu, P.; Kirkpatrick, R.J.; Poe, B.; McMillan, P.F.; Cong, X. Structure of calcium silicate hydrate (C-S-H): Near- mid-, and far-infrared spectroscopy. *J. Am. Ceram. Soc.* **1999**, *82*, 742–748. [[CrossRef](#)]
55. Carrasco, L.F.; Martín, D.T.; Morales, L.; Ramírez, S.M. *Infrared Spectroscopy in the Analysis of Building and Construction Materials*; IntechOpen: London, UK, 2012. [[CrossRef](#)]
56. Hughes, T.L.; Methven, C.M.; Jones, T.G.; Pelham, S.E.; Fletcher, P.; Hall, C. Determining cement composition by Fourier transform infrared spectroscopy. *Adv. Cem. Based Mater.* **1995**, *2*, 91–104. [[CrossRef](#)]
57. Saad, A.M.; Saleh, A.-B.A.; Al-Kadri, F.A.; Babaqi, A.S.; Basissa, A.A.; Abo-El-Enein, S.A. Studies of Surface Area and Pore Structure on Portland Cement Produced in Bajil and Amran, Yemen. *Sultan Qaboos Univ. J. Sci.* **2008**, *13*, 13–25. [[CrossRef](#)]
58. Moghaddam, F.; Sirivivatnanon, V.; Vessalas, K. The effect of fly ash fineness on heat of hydration, microstructure, flow and compressive strength of blended cement pastes. *Case Stud. Constr. Mater.* **2019**, *10*, e00218. [[CrossRef](#)]
59. Qudoos, A.; Kim, H.G.; Atta-ur-Rehman; Jeon, I.K.; Ryou, J.-S. Influence of the particle size of wheat straw ash on the microstructure of the interfacial transition zone. *Powder Technol.* **2019**, *352*, 453–461. [[CrossRef](#)]
60. Bose, B.; Davis, C.R.; Erk, K.A. Microstructural refinement of cement paste internally cured by polyacrylamide composite hydrogel particles containing silica fume and nanosilica. *Cem. Concr. Res.* **2021**, *143*, 106400. [[CrossRef](#)]
61. Bodor, E.; Skalny, J.; Brunauer, S.; Hagymassy, J., Jr.; Yudenfreund, M. Pore structures of hydrated calcium silicates and Portland cements by nitrogen adsorption. *J. Colloid Interface Sci.* **1970**, *34*, 560–570. [[CrossRef](#)]